

Nanoscale

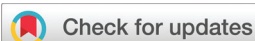
rsc.li/nanoscale



ISSN 2040-3372

PAPER

Jisen Wen, Sang-Shin Lee *et al.*
Switchable optical trapping based on vortex-pair beams
generated by a polarization-multiplexed dielectric
metasurface


 Cite this: *Nanoscale*, 2023, **15**, 17364

Switchable optical trapping based on vortex-pair beams generated by a polarization-multiplexed dielectric metasurface†

 Hongliang Li, ^{a,b} Jisen Wen,^{*c} Song Gao, ^d Duk-Yong Choi, ^e Jin Tae Kim ^f and Sang-Shin Lee ^{*a,b}

Optical trapping is a state-of-the-art methodology that plays an integral role in manipulating and investigating microscopic objects but faces formidable challenges in multiparticle trapping, flexible manipulation, and high-integration applications. In this study, we propose and demonstrate a switchable optical scheme for trapping microparticles incorporating disparate vortex-pair beams generated by a polarization-multiplexed metasurface. The miniaturized all-dielectric metasurface, which comprises an array of titanium dioxide nanoposts, was manufactured and characterized to provide polarization-tuned two-fold vortex-pair beams. The profiles of the created vortices can be flexibly tailored by adjusting the combination of topological charges and the separation among phase singularities. Under transverse electric polarized light conditions, a vortex-pair beam with opposite topological charge combinations traps a single microparticle within one beam spot, while under transverse magnetic polarization conditions, two microparticles are captured simultaneously by a vortex-pair beam with the same topological charge signs. The proposed switchable trapping scheme (incorporating a vortex-pair light beam) is expected to feature enhanced integration and flexible manipulation of multiple particles with potential applications in biophysics, nanotechnology, and photonics.

 Received 17th August 2023,
 Accepted 9th October 2023

DOI: 10.1039/d3nr04125e

rsc.li/nanoscale

1. Introduction

Since A. Ashkin proposed the concept of optical trapping in the 1970s, optical tweezers have been serving a vital role in various fields, such as biology, physics, and chemistry, whereby tiny objects can be manipulated in a noncontact, non-invasive, and high-precision manner.^{1,2} The optical trapping of micro-nano particles is based on light beams that exert gradient (or dipole) and scattering forces (or radiation pressure).^{3,4} The former is relevant to the gradient of light intensity and the latter to the Poynting vector. The realization of a non-destructive scheme for the optical trapping of a pre-

defined number of particles has been a long-sought mission. Toward this end, a focused Gaussian beam played a paramount role in effectuating optical trapping processes,^{5,6} however it is only capable of enabling the precise manipulation and confinement of a single minuscule entity, such as a nanoscale particle or cell. A vortex beam, resorting to the helical rotation of the wavefront, is capable of inducing a plethora of remarkable phenomena like rotating a bead, further enriching the domain of optical trapping.⁷⁻⁹ Yet, a constant, single-orbital angular momentum carried by the vortex beam renders it unsuitable for optical manipulation and information transport, thus limiting its potential applications toward the study of cell interactions or the assembly of micro-devices. Therefore, the higher flexibility and degrees of freedom offered by structured beams exhibiting customized phases, amplitudes, and polarizations have attracted tremendous attention in optical trapping.¹⁰⁻¹² In particular, the implementation of such structured beams is primarily based on a spatial light modulator (SLM) for adjusting the phase of light, which offers real-time flexibility and controllability.¹³ Nevertheless, the SLM has demerits in terms of bulkiness, low integration, and thermal sensitivity. Consequently, a compact, highly integrated, and thermally stable beam generator should be urgently developed.

Metasurfaces, alluding to two-dimensional arrays of ultrathin subwavelength-scale unit cells, are known to control the

^aDepartment of Electronic Engineering, Kwangwoon University, Seoul, 01897, South Korea. E-mail: slee@kw.ac.kr

^bNano Device Application Center, Kwangwoon University, Seoul, 01897, South Korea

^cResearch Center for Intelligent Chips and Devices, Zhejiang Lab, Hangzhou, 311121, China. E-mail: wenjisen@zju.edu.cn

^dSchool of Information Science and Engineering, Shandong Provincial Key Laboratory of Network Based Intelligent Computing, University of Jinan, Jinan, Shandong, 250022, China

^eDepartment of Quantum Science and Technology, Research School of Physics, Australian National University, Canberra, ACT 2601, Australia

^fQuantum Technology Research Department, Electronics and Telecommunications Research Institute, Daejeon, 34129, South Korea

† Electronic supplementary information (ESI) available. See DOI: <https://doi.org/10.1039/d3nr04125e>

amplitude, phase, and polarization of light,^{14–16} potentially paving an avenue to deal affordably with polarization manipulation, beam shaping, and aberration correction. Recently, various configurations of metasurfaces have been extensively researched given their conspicuous electromagnetic features, stable performance, and diverse functionalities, encompassing advanced optical communications,^{17,18} ultrathin flat lenses,^{19,20} various sensors,^{21,22} and particle trapping devices.^{23,24} The optical trapping can be flexibly tailored by imposing a specific phase distribution on the metasurfaces.^{25,26} Li *et al.* theoretically verified the possibility of taking advantage of metasurfaces to demonstrate optical tweezers and wrenches.²⁵ Li *et al.* experimentally realized the trapping and dragging of a silicon dioxide bead by a focused Gaussian beam.²⁶ Regarding highly integrated devices, Suwannasopon *et al.* succeeded in integrating metasurfaces with liquid crystals to construct an optical tweezer.²⁷ Plidschun *et al.* proved the feasibility of meta-fiber-based optical trapping.²⁸ These previous studies highlighted the seminal potential of metasurface devices highly integrated with conventional optics for optical trapping applications; however, the metasurface-mediated optical tweezers were mainly designed to drag individual beads. In this aspect, a substantially miniaturized versatile optical tweezer is categorically necessitated from the perspective of flexibly handling multiple particles at a time.

In this study, we propose and demonstrate a polarization-multiplexed all-dielectric metasurface that can generate a set of vortex-pair beams and demonstrate switchable optical trapings. The proposed monolayer metasurface, incorporating a series of titanium dioxide (TiO₂) nanoposts on a silica substrate, was created precisely *via* lithography technology, TiO₂ atomic layer deposition, and plasma etching. We systematically evaluated the creation and evolution of vortex-pair beams in terms of the separation between their phase singularities. It was found that the experimental characterization had a high degree of consistency with the simulation results. As a proof-of-concept, under transverse electric (TE) polarized light conditions, when the vortex-pair beam has opposite signs in two topological charges, only one optical trapping exists and can trap one microparticle. Conversely, when the incident light is transformed to transverse magnetic (TM) light, two microparticles can be trapped by the metasurface-based vortex-pair beam with the same topological charge sign. The demonstrated metasurface providing polarization-sensitive structured beams is categorically expected to facilitate improved light-trapping integration and flexibility, potentially enriching the multi-particle manipulation approach.

2. Theory and results

2.1 Polarization-multiplexed all-dielectric metasurface based on vortex-pair beam

A vortex-pair beam is a type of structured light beam that incorporates a pair of vortices with the same or opposite topological

charges in the phase plane.^{29–32} Each vortex stems from a region where the phase of the electromagnetic field rotates with respect to a phase singularity, thus creating a helical wavefront.^{33,34} The sign of the two topological charges determines the direction of phase rotation. Both the vortex and vortex-pair beams are principally characterized by their angular momentums. Their wavefronts have spiral shapes and deliver spin and orbital angular momentums, which can be harnessed to manipulate microparticles. Depending on the combination of topological charges and their signs, the vortex behavior can be significantly differentiated. To distinguish the types of beams more effectively, we first devised two simple vortex phases corresponding to topological charges of $m = -1$ and $m = 1$,^{35,36} as shown in Fig. 1(a). For the vortex beam, negative and positive topological charges lead to a single, spatially varying spiral-shaped beam phase that increases from 0 to 2π in the counterclockwise (yellow arrow) and clockwise directions (green arrow), respectively. Fig. 1(b) shows two examples of vortex-pair phases in response to the topological charges of $m_1 = -m_2 = 1$ and $m_1 = m_2 = 1$, giving rise to spirals in the opposite or same directions, respectively, in response to phase variations from 0 to 2π . In the meantime, the amount of separation between the two vortices can be set by a structural parameter a , thus referring to the offset with respect to the center at the phase plane. As shown in Fig. 1(c), to facilitate two-fold optical trapping, we capitalized on a polarization-multiplexed all-dielectric metasurface to establish vortex-pair beams with the same and opposite signs of topological charges. Specifically, under incident TE polarization aligned along the x -axis, we aimed to embody a vortex-pair beam with topological charges with opposite signs, thereby rendering a single vortex-trapping scheme. For incident TM polarization along the y -axis, the phase profile associated with the metasurface was tailored to choose topological charges of the same sign so that an optical field could be developed to induce a strong transverse gradient force to trap concurrently pairs of microparticles. A team of vortices is highly expected to exhibit more flexible and versatile electromagnetic manipulation according to various parameters, such as topological charge signs, compared with the case of a simple vortex phase, as asserted by the examples of the intensity distribution in Fig. 1(d). The intensity distribution of two vortex-pair beams is inspected based on several structural parameters and phase profiles as delineated in Fig. 1(b). When they have opposite topological charge signs, the two vortices merge to form a single, strong spot similar to that of a focused Gaussian beam. Meanwhile, when the vortices share the same topological charge signs and magnitudes, a more complicated distribution incorporating double strong spots is produced. The white arrow depicted in the figure represents the Poynting vector, which symbolizes the direction of power flow.

Regarding the targeted metasurface, an adequate phase control method should be secured to implement the phase profile. Toward this end, the propagation phase technique is exploited to embody the proposed polarization-tailored optical-trapping scheme.^{37,38} A suite of polarization-sensitive

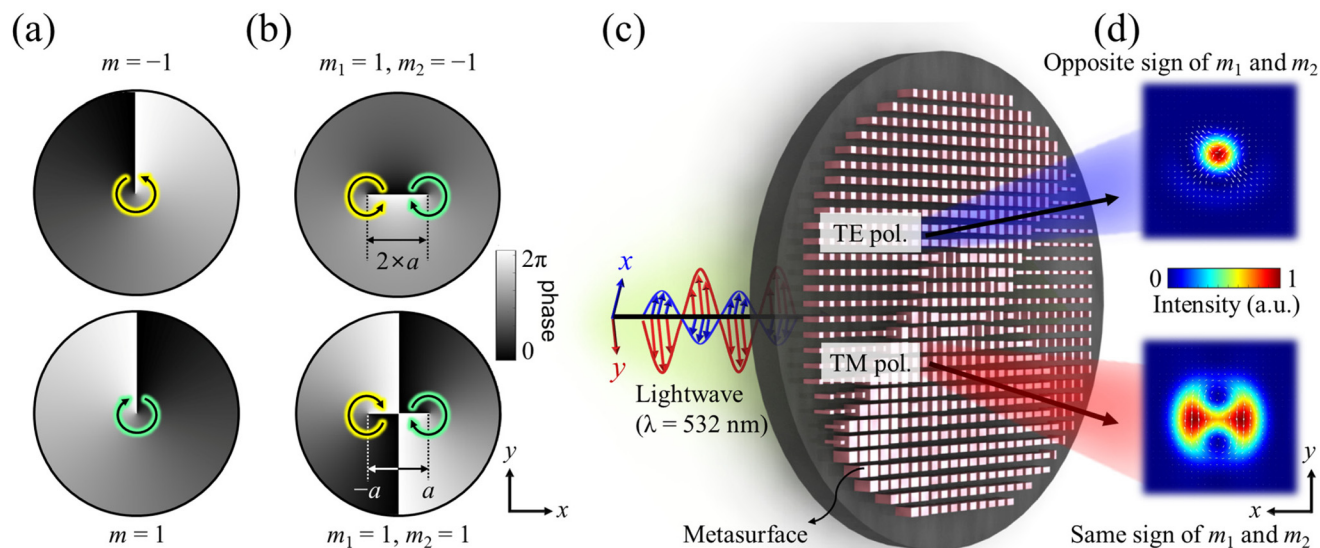


Fig. 1 (a) Phase profiles of an optical vortex with topological charges of $m = -1$ and $m = 1$. (b) Phase profiles of an optical vortex-pair with a dual topological charge corresponding to $m_1 = 1, m_2 = -1$ and $m_1 = 1, m_2 = 1$. (c) Schematic of the proposed polarization-multiplexed dielectric metasurface enabling switchable optical trapping. (d) The corresponding intensity profiles of the vortex-pair beam at the focal plane of the objective lens (OL).

TiO₂ nanoposts is adopted to construct a metasurface device operating at a wavelength of 532 nm. Fig. 2(a) shows side-view schematics of the dielectric meta-atoms constituting the proposed metasurface. The refractive index (n) of TiO₂ is measured to be 2.38 by ellipsometry (J.A. Woollam M2000D), while the glass substrate has $n = 1.45$. The transmission amplitude and phase of the meta-atoms under incident light conditions for TE and TM polarizations were numerically deter-

mined using a simulation tool, FDTD (finite-difference time-domain) Solutions (Ansys/Lumerical 2023R1, USA) simulation tool. The period (p) of the lattice was 350 nm along the x - and y -axes, and the height (h) of the nanoposts was 500 nm. A set of nanopillars with different cross-sectional dimensions of width (w) and length (l), which can invoke a polarization-dependent phase shift, was arranged in accordance with a square lattice. A 2π phase shift and a high transmittance ($T >$

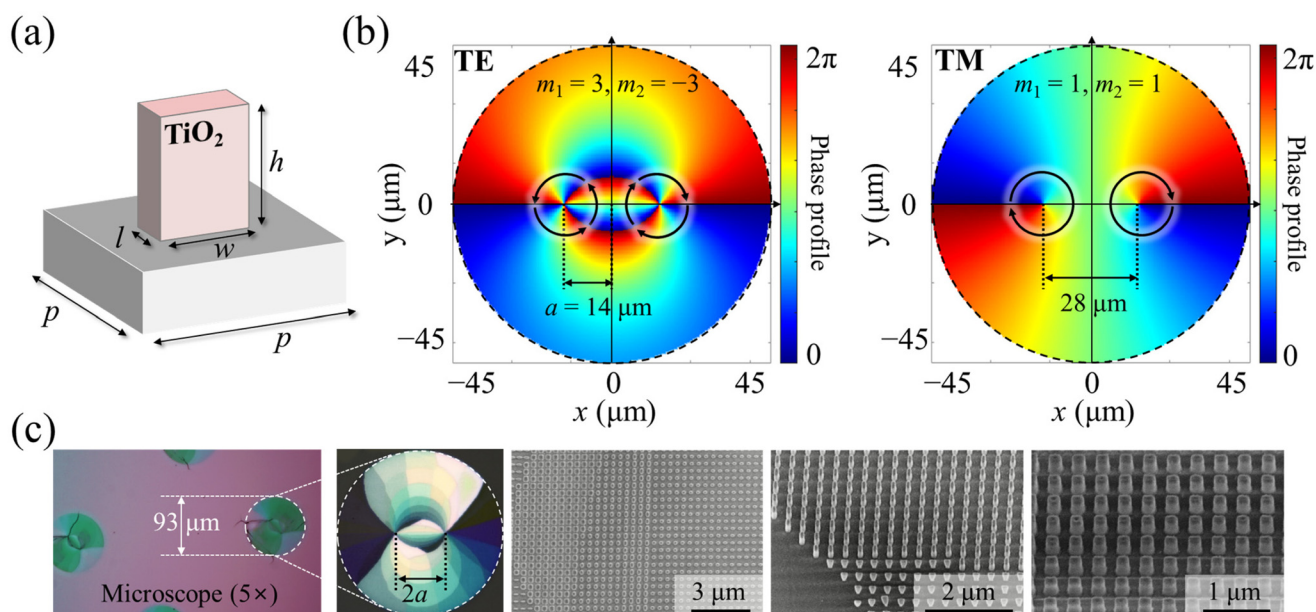


Fig. 2 (a) Configuration of the designed TiO₂ nanopost formed on a silica substrate constituting the meta-atoms. (b) Calculated relative phase profiles for the TE and TM polarization. (c) Optical microscope image of the manufactured metasurface device on a glass substrate and scanning electron microscope images of the constituting meta-atoms of the metasurface observed at different scales.

0.8) were respectively obtained under the TE and TM polarization conditions, as shown in Fig. S1(a) and (b) in ESI.† Finally, a group of 8×8 highly efficient nanoposts, independently allowing for full 2π -phase modulations for both TE and TM polarizations, was selected to make up the metasurface, as indicated by the black stars. The vortex-pair phase of the proposed metasurface can be expressed as

$$\phi = \arctan \left[\frac{\text{Im}(E_\phi)}{\text{Re}(E_\phi)} \right],$$

where E_ϕ refers to the light field of a vortex-pair beam at the initial plane³¹ and was calculated as

$$E_\phi(x, y) = \left[\frac{x - a + jy}{\sqrt{(x - a)^2 + y^2}} \right]^{m_1} \left[\frac{x + a + jy}{\sqrt{(x + a)^2 + y^2}} \right]^{m_2}.$$

Here m_1 and m_2 are integer topological charges, a is the off-axis distance of each vortex, and (x, y) allude to the coordinates corresponding to the center of a unit cell constituting each metasurface. The phase formula adopted to generate the vortex-pair beam is based on an artificially designed phase function.³² Unlike vortex beams, vortex-pair beams are not rotationally symmetric and their properties are subject to the magnitude and sign of topological charges thereof. The influence of the parameters, including m_1 , m_2 , and a on the phase profiles has been rigorously conducted, as described in Fig. S2 (ESI†). To guarantee that the desired phase shift could be accurately substantiated by the selected meta-atoms, an excessively large magnitude of topological charges should be circumvented to relax phase changes. Furthermore, it is advisable to set the parameter a to values corresponding to 0.15 to 0.25 times the metasurface diameter (d), thus appropriately setting apart the topological charges. In this context, topological charge combinations corresponding to $m_1 = -m_2 = 3$ and $m_1 = m_2 = 1$ have been chosen to execute the proposed twofold optical trapping, with a fixed at $14 \mu\text{m}$. The calculated phase profiles of the developed metasurface for the two polarizations are portrayed in Fig. 2(b). The proposed metasurface was made of TiO_2 on a glass substrate using electron beam lithography (for details, see the Methods section). Top and perspective views of the fabricated structure are shown in Fig. 2(c).

To validate the operation mechanism of the proposed metasurface, rigorous simulations were conducted to assess the evolution of the transmitted light field with the aid of FDTD solutions. Fig. 3(a) shows the x - z crossing view of the beam propagation for the incident TE and TM polarization. The vortex beam exhibits polarization-contingent spots according to the topological charge signs thereof. A single intense beam spot was obtained for the opposite-sign case, while double intense beam spots were obtained for the same-sign case. The x - y crossing views of the beam propagation displayed in Fig. 3(b) show that (as expected) the shape of the transmitted beam spot for the same metasurface is subject to polarization-tuned phase distributions. To assess the fabricated metasurface, an experimental setup is deployed as shown in Fig. 3(c).

First, a commercial laser at a center wavelength of 532 nm was utilized as the light source. A half-wave plate (HWP_1) and linear polarizer (LP) were employed to control the power of an emitted Gaussian beam, which was directed through HWP_2 to adjust its polarization direction before reaching the metasurface. The metasurface was placed on an adjustable platform, while the evolution of the vortex-pair beam was monitored with a charge-coupled device camera. The calculated far-field beam profiles of the vortex-pair beams (observed at $z = 5 \text{ cm}$) are compared with the experimental profiles, as illustrated in Fig. 3(d) and (e). For topological charges of the same magnitude but opposite signs, as in the case of $m_1 = -m_2 = 3$, the vortex-pair beam was focused into a single bright spot to engender sharp and strong intensity peaks, thus inducing a strong transverse gradient force which traps single microparticles. In contrast, in the case of two equal positive topological charges, as in the case of $m_1 = m_2 = 1$, the vortex-pair was focused on two bright spots; each of these had sharp and high-intensity peaks that invoked a strong transverse gradient force facilitating the seizing of multiple microparticles. Subsequently, the impact of the size of the incident light beam on the vortex-pair beam was explored in ESI (Fig. S3†). It is observed that when the spot of the incident Gaussian beam exceeds the footprint of the metasurface, the beam evolution is rarely affected. The polarization-dependent transmission of the proposed metasurface was also explored by monitoring the beam power along the propagation position. The transmissions, calculated by measuring the power before and behind the metasurface, were 84.0% and 83.9% for the TE and TM polarizations, respectively, which are in close agreement with the corresponding simulated efficiencies of 89.1% and 88.6%, underpinning the high-efficiency characteristics of TiO_2 -based metasurface devices.

2.2 Metasurface characterization and optical tweezers application

Metasurfaces with specific angular momentum have been extensively perceived as a popular vehicle in optical tweezer applications thanks to their compact, ultrathin platform, and high-integration characteristics.²³ As a proof-of-concept, a custom-built test setup was established to probe into the feasibility of switchable optical trapping mediated by the proposed polarization-sensitive dielectric metasurface, as shown in Fig. 4(a) and as detailed in the Methods section. The process of trapping dielectric microbeads based on the proposed vortex-pair beam is analytically expounded in the ESI (Fig. S4†). The two relevant groups of experimental demonstration can be viewed in Videos S1–S4 (ESI†). We extracted two separate 30 s videos under TE and TM polarization conditions to assess the stability of vortex-pair-trapped microbeads in the optical beam. Each video was uniformly divided into 300 frames; the first 15 s (150 frames) captured the stage movement along the x -axis, and the subsequent 15 s captured the movement along the y -axis, as depicted by the blue and red backgrounds in Fig. 4(b) and (c), respectively. Considering that the particles remained securely confined throughout the entire

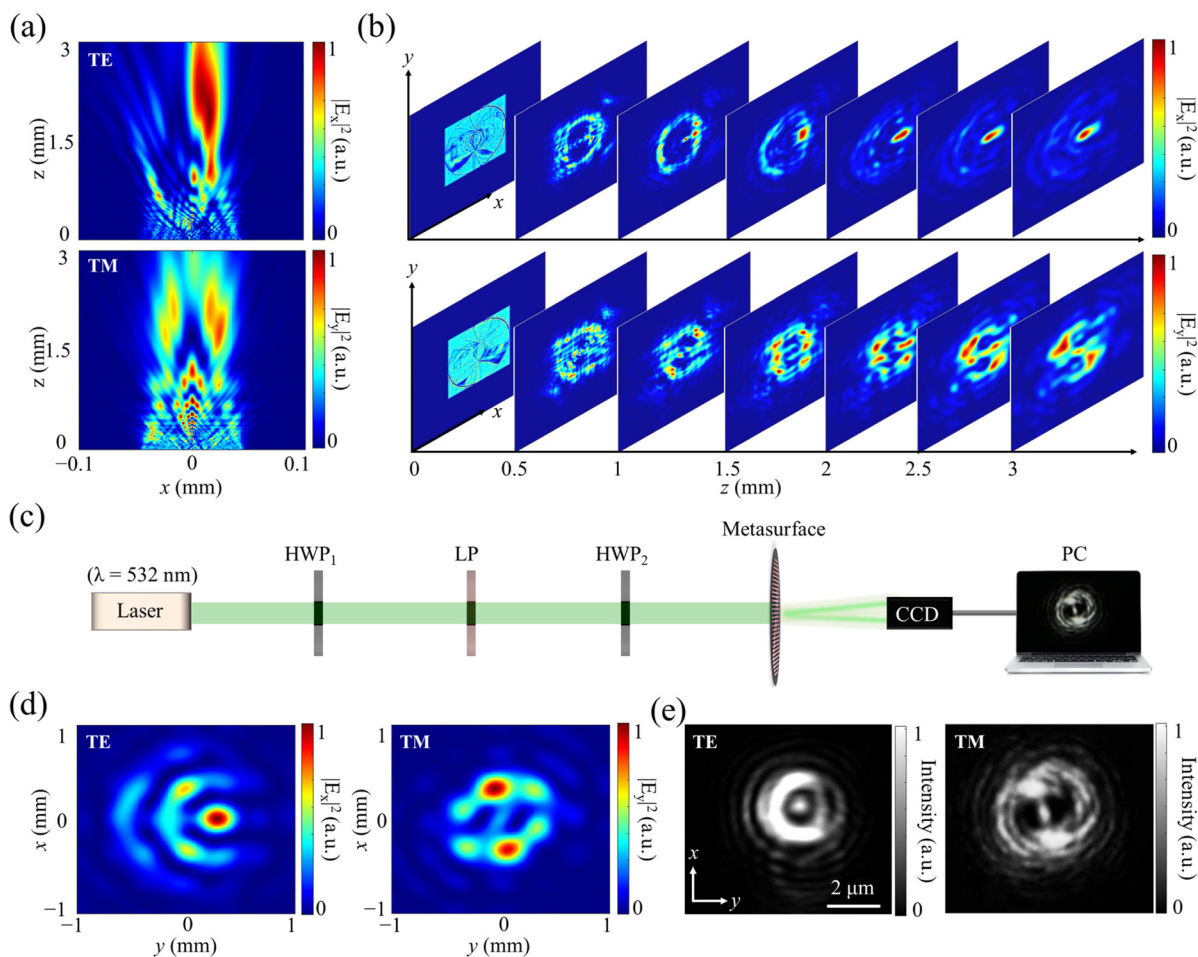


Fig. 3 (a) E-Field ($|E_x|^2$ and $|E_y|^2$) distributions in the xz -plane of the transmitted beam in response to normally incident TE- and TM-polarized light, respectively. (b) Evolution of the $|E_x|^2$ and $|E_y|^2$ distributions under the corresponding polarization conditions in terms of the propagation distance, which ranged from $z = 0$ to 3000 μm in 0.5 mm steps. (c) Schematic of the experimental setup for characterizing the metasurface. (d) Calculated far-field and (e) experimentally observed intensity profiles of the vortex-pair beams with topological charge combinations of $m_1 = 3$, $m_2 = -3$ and $m_1 = 1$, $m_2 = 1$ for the TE and TM polarizations, respectively. The white scale bar is tantamount to 2 μm .

video without escaping, we then investigated the stability of the center position of the vortex-pair beam because the trapped beads were nearly concealed within the spot. In the TE case, the optical vortex beam efficiently trapped single particles with variances along the x - and y -axes corresponding to approximately 0.13 and 0.05 μm^2 , respectively. It is crucial to emphasize that when the sample stage is displaced along the x -axis, the variance in the x -direction ($\text{var}_{x1} = 0.16 \mu\text{m}^2$) increases unavoidably to surpass the variance in the y -direction ($\text{var}_{y1} = 0.039 \mu\text{m}^2$). However, when it comes to the movement along the y -axis, the variance in the y -direction tends to increase ($\text{var}_{y2} = 0.06 \mu\text{m}^2$) while the variance in the other direction ($\text{var}_{x2} = 0.099 \mu\text{m}^2$) is deemed to decrease. Under TM polarization conditions, we initially derived the center positions corresponding to the two bright spots as shown in Fig. S5.† The center position was subsequently checked to perform a variance analysis. Similarly, during the displacement of the sample plate, the variance along the particular direction exhibited a slight increase compared with the var-

iance in the orthogonal direction owing to particle jittering. The total variance along the x - and y -directions were respectively found to be approximately equal to 0.019 and 0.034 μm^2 . The achieved outcomes underpin the robust confinement and stability of the trapped particles throughout the stage movement in both the TE and TM cases. The small variance values along both x - and y -directions signify that the optical tweezers stably retain the bead during the experiment, thus supporting the reliability and precision of the proposed trapping scheme.

To demonstrate further the convenience and performance of the tunable optical tweezers mediated by the polarization-multiplexed metasurface, a suite of typical camera snapshots of the trapped microbead are presented in Fig. 5. For the topological charge combination of $m_1 = 1$ and $m_2 = 1$, the metasurface under light illumination of TM polarization gives rise to two bright spots with sharp and high-intensity peaks, exerting strong transverse gradient forces which are suitable for seizing microparticles, as depicted in Fig. 5(a). The two microparticles—initially arranged along the y -axis—are displaced to be verti-

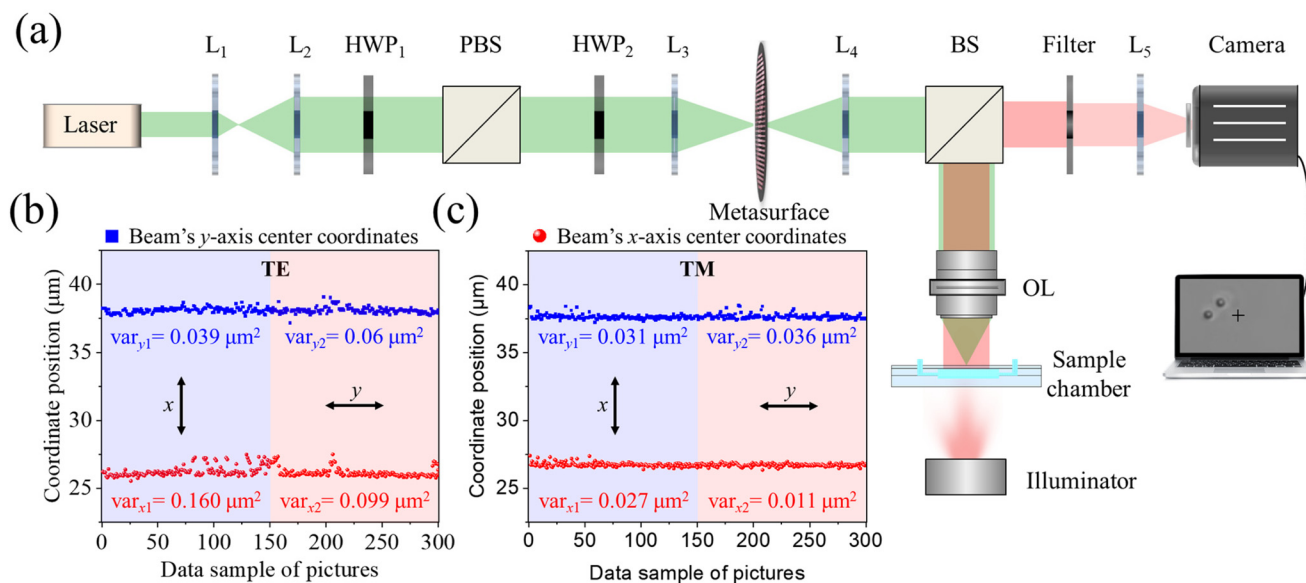


Fig. 4 (a) Schematic of the optical trapping setup (L, lens; PBS, polarizing beam splitter; BS, beam splitter). The center position of vortex-pair beams under (b) TE and (c) TM polarization conditions was measured to quantitatively analyze the stability of optical tweezers-trapped microbeads.

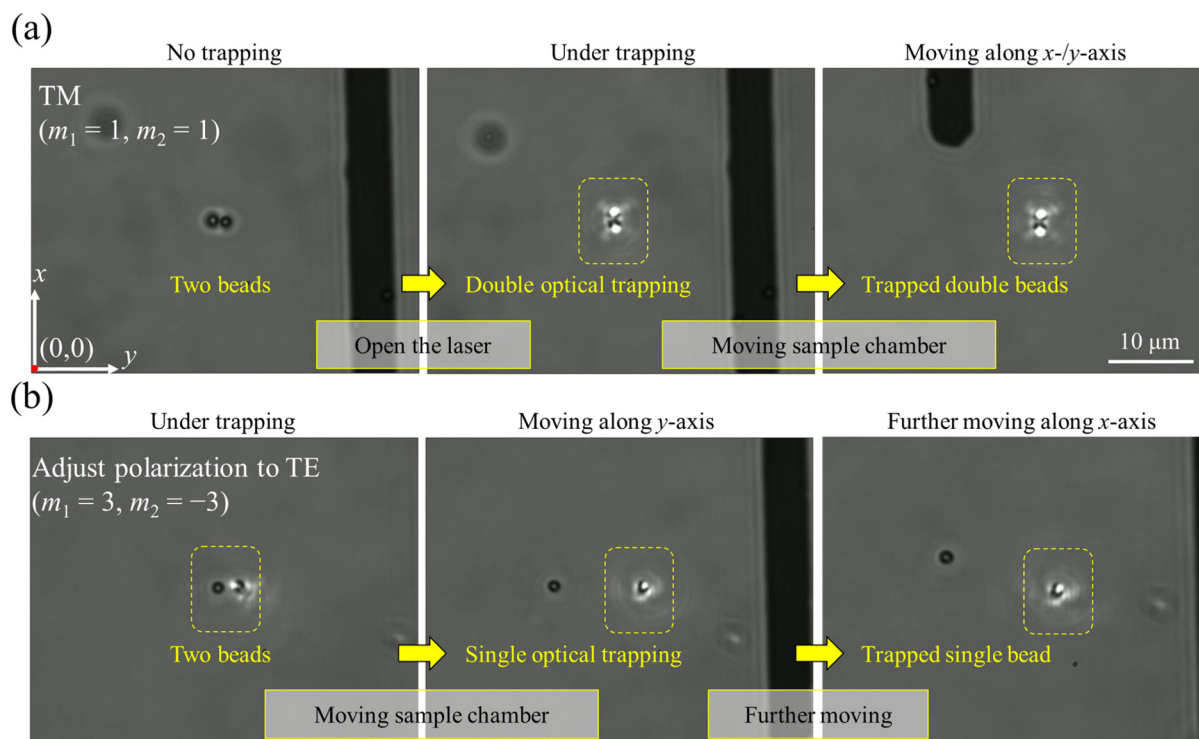


Fig. 5 Camera snapshots of the spherical microparticles which are being optically trapped by the focused vortex-pair beam under (a) TM and (b) TE polarization conditions, where the dashed boxes mark the regions wherein the irradiated light field reside.

cally arranged along the x -axis as a result of being irradiated by the two strong spots belonging to the vortex-pair beam. It is observed that even when the sample plate is displaced using a high-resolution stage, the two microparticles are firmly held in the transverse xy -plane with each particle occupying the posi-

tion of either of the light spots. However, in the case of $m_1 = 3$ and $m_2 = -3$, as shown in Fig. 5(b), the phase profile of the beam yields a single strong optical trap. Herein, only one of the two spherical microparticles is stably kept in place during the displacement of the sample plate. The microbead which is

not exposed to the focused light field is hardly trapped and freely drifts away alongside the sample plate. The black columnar patterns (as observed in Fig. 5) denote the reference lines engraved on the sample plate, serving as an indicator showing the distance traversed by the stage. It is noted that the black microbeads as observed in the figures and videos do not necessarily reflect their actual dimensions, which is owing to light scattering.

It is notable that the two sets of pictures reveal the action of optical trapping alongside the vortex-pair beam in tight focus mode, as depicted in Fig. 5. In this scenario, the vortex-pair beam is passed through an OL to boost the beam power and corresponding gradient force before taking hold of the micro-particles. Hence, to gain further insights into the characteristics of the vortex-pair beam in the tight focus mode, the beams going through a high-NA OL were assessed with the help of MATLAB (version R2021b, MathWorks, Natick, MA, USA), as shown in the schematic in Fig. S6.† Herein, the symbol z_{OL} denotes the distance between the location of vortex-pair beams in the tight focus mode and the sample chamber, which is positioned at the focal length ($z_{OL} = 0$). As shown in Fig. 6(a), when the vortex-pair beam assumes two identical topological charges ($m_1 = m_2 = 1$), the intensity distribution of the beam remains invariant along the propagation direction except for the rotation of the entire pattern and the contraction of the two vortices in the tight focus mode.³² Eventually, the beam tends to forge a couple of bright spots at the focal plane, which symmetrically evolve along the x - and y -axes to facilitate the optical trapping of two microparticles. For the case of opposite topological charges ($m_1 = 3$ and $m_2 = -3$), the two elemental vortices tend to be mutually attractive during propagation. When the paired vortices are positioned in close proximity, they may undergo both collision and destructive interference and they eventually vanish.³¹ Finally, the intensity distribution at the focal plane is mostly symmetrically centered along the y -axis, and only a single bright spot is activated to hold a microparticle, as shown in Fig. 6(b).

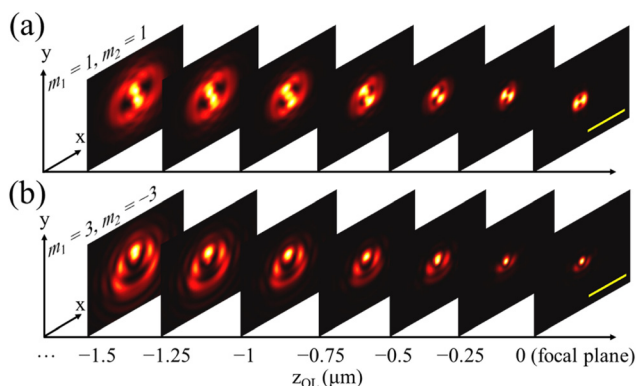


Fig. 6 Calculated intensity profiles of the vortex-pair beam propagating through a high-NA OL for (a) $m_1 = m_2 = 1$ and (b) $m_1 = -m_2 = 3$. The yellow scale bar corresponds to $2\ \mu\text{m}$ (NA: numerical aperture).

3. Discussion and conclusions

Our study focused on a successful demonstration of vortex-pair-based optical trapping of a single and a pair of beads by polarization manipulation. However, it should be noted that the use of a vortex-pair beam based on metasurface is constrained to deal with (at most) two particles. To mitigate this limitation, other alternative schemes that capitalize on highly complex structured light, encompassing Ince–Gaussian beams,¹³ autofocusing Airy beams,³⁹ azimuthally polarized beams,⁴⁰ may be potentially used to trap more particles. Further research and development in this direction should be essential to facilitate multiparticle trapping.

In summary, a polarization-multiplexed metasurface was successfully constructed to generate two-fold vortex-pair beams, enabling switchable optical trapping of particle numbers. The all-dielectric metasurface was successfully processed and characterized; it exhibited a high transmission efficiency ($\sim 84\%$) at a wavelength of 532 nm. The performance of the vortex-pair beams was well implemented, successfully characterized, and matched well with the theoretical and simulated predictions. As a proof-of-concept, we conducted experimental examinations of two types of optical trapping with distinct characteristics—single-particle trapping (topological charge of $m_1 = 3$, $m_2 = -3$) and two-particle trapping ($m_1 = 1$, $m_2 = 1$)—due to the transverse gradient force generated by the strong light spot at the focal plane of the OL. The prominent advantages, such as a miniaturized footprint, two-fold optical trapping, and polarization controllability, allow the realized metasurface to promote the development of advanced optical tweezers in multiparticle manipulations.

4. Experimental

4.1 Metasurface characterization and optical tweezer applications

The designed all-dielectric metasurface was practically manufactured, as delineated in Fig. S7.† A glass substrate (thickness = 1 mm) was cleaned and coated with an electron beam resist (ZEP 520A, Zeon, Japan). Subsequently, electron-beam lithography based on Raith150 was applied to create a pattern associated with the designed metasurface. The baking process was keenly related to the sidewall profile of the resist, alongside the baking temperature and time. It was disclosed through several processes; as the baking temperature increased from 130 to 135 °C (1 min), the sidewall angle about the nanostructures was altered from negative to positive, thereby minimizing the geometrical shadowing effect.^{41,42} Distortion in the pattern's dimensions and shape caused by the proximity effect was minimized by taking advantage of high-electron beam energy (30 kV) and a small duty ratio of holes. The patterned holes were filled up using a TiO_2 layer grown with atomic layer deposition. TiO_2 blanket etching was subsequently conducted *via* CHF_3 plasma to reach the resist surface. Finally, the electron-beam resist was removed using oxygen plasma. The com-

pleted metasurface was inspected using optical and scanning electron microscopy. The prepared metasurface and its structural profile are displayed in Fig. 2(c). To replicate the target phase profile, the meta-atom period was set at 350 nm to provide denser meta-atoms.

4.2 Measurement setup for the metasurface-based optical tweezer experiment

As shown in Fig. 4(a), the spot of the incident Gaussian beam is initially enlarged to 1.5 mm in diameter *via* lenses L_1 and L_2 . The beam is then passed through HWP₁ and a polarizing beam splitter to deliver moderate beam power. The optical path was routed *via* a plane mirror and the reflected light was passed through HWP₂ to control its polarization. The light was then focused on the metasurface using lens L_3 . Finally, the microsphere sample plate was irradiated with light passing through lens L_4 , beam splitter, and an OL (CFI Achromat, 100 \times) with a working distance of 0.23 mm and an NA of 1.25. Additionally, auxiliary components encompassing an illuminator light-emitting diode, a bandpass filter, L_5 , and a camera (TouPCam I3CMOS, TouPTek Photonics), were incorporated into the setup to enhance visibility and efficiently locate the beam spot. Spherical polypropylene microparticles (BaseLine ChromTech Research Centre, Tianjin, China) with a diameter of 1 μm were used.

Author contributions

Hongliang Li: conceptualization (lead); data curation (lead); formal analysis (lead); investigation (lead); methodology (lead); visualization (lead); writing – original draft (lead); writing – review & editing (lead). Jisen Wen: investigation (equal); formal analysis (equal); validation (lead); data curation (equal); writing – original draft (equal); supervision (equal); writing – review & editing (equal). Song Gao: formal analysis (supporting); methodology (equal); writing – original draft (equal); supervision (equal). Duk-Yong Choi: resources (equal); writing – review & editing (equal). Jin Tae Kim: writing – review & editing (supporting). Sang-Shin Lee: supervision (equal); funding acquisition (lead); writing – review & editing (lead). Thanks to Binjie Gao of Zhejiang University for his help and discussion in the optical tweezer experiments.

Conflicts of interest

There are no conflicts to declare.

Acknowledgements

This work was supported by the National Research Foundation of Korea (2018R1A6A1A03025242), Ministry of Science and ICT, Republic of Korea (2020R1A2C3007007), Kwangwoon University (in 2023), National Natural Science Foundation of China (62005095), and Shandong Provincial Natural Science

Foundation (ZR2020QF105). Metasurface nanofabrication was performed at the ACT node of the Australian National Fabrication Facility.

References

- 1 A. Ashkin, Acceleration and Trapping of Particles by Radiation Pressure, *Phys. Rev. Lett.*, 1970, **24**, 156.
- 2 L. Paterson, M. P. MacDonald, J. Arlt, W. Sibbett, P. E. Bryant and K. Dholakia, Controlled rotation of optically trapped microscopic particles, *Science*, 2001, **292**, 912–914.
- 3 M. L. Juan, M. Righini and R. Quidant, Plasmon nano-optical tweezers, *Nat. Photonics*, 2011, **5**, 349–356.
- 4 C. J. Bustamante, Y. R. Chemla, S. Liu and M. D. Wang, Optical tweezers in single-molecule biophysics, *Nat. Rev. Dis. Primers*, 2021, **1**, 25.
- 5 A. I. Bunea and J. Glückstad, Strategies for optical trapping in biological samples: Aiming at microrobotic surgeons, *Laser Photonics Rev.*, 2019, **13**, 1800227.
- 6 C. Hosokawa, T. Tsuji, T. Kishimoto, T. Okubo, S. N. Kudoh and S. Kawano, Convection dynamics forced by optical trapping with a focused laser beam, *J. Phys. Chem. C*, 2020, **124**, 8323–8333.
- 7 W. Lamperska, J. Masajada and S. Drobczyński, Microscale solute flow probed with rotating microbead trapped in optical vortex, *Exp. Fluids*, 2021, **62**, 128.
- 8 A. T. O'neil, I. MacVicar, L. Allen and M. J. Padgett, Intrinsic and extrinsic nature of the orbital angular momentum of a light beam, *Phys. Rev. Lett.*, 2002, **88**, 053601.
- 9 S. Shetty, S. Bharati, S. Chidangil and A. Bankapur, Optical trapping and micro-Raman spectroscopy of functional red blood cells using vortex beam for cell membrane studies, *Anal. Chem.*, 2021, **93**, 5484–5493.
- 10 A. Forbes, M. de Oliveira and M. R. Dennis, Structured light, *Nat. Photonics*, 2021, **15**, 253–262.
- 11 C. He, Y. Shen and A. Forbes, Towards higher-dimensional structured light, *Light: Sci. Appl.*, 2022, **11**, 205.
- 12 J. Wang and Y. Liang, Generation and detection of structured light: a review, *Front. Phys.*, 2021, **9**, 688284.
- 13 Y. Yang, Y. X. Ren, M. Chen, Y. Arita and C. Rosales-Guzmán, Optical trapping with structured light: a review, *Adv. Photonics*, 2021, **3**, 034001–034001.
- 14 Y. Yuan, S. Sun, Y. Chen, K. Zhang, X. Ding, B. Ratni, Q. Wu, S. N. Burokur and C.-W. Qiu, A fully phase-modulated metasurface as an energy-controllable circular polarization router, *Adv. Sci.*, 2020, **7**, 2001437.
- 15 S. Wang, P. C. Wu, V. C. Su, Y. C. Lai, C. Hung Chu, J. W. Chen, S.-H. Lu, B. Xu, C.-H. Kuan, T. Li, S. Zhu and D. P. Tsai, Broadband achromatic optical metasurface devices, *Nat. Commun.*, 2017, **8**, 187.
- 16 G. Kim, S. Kim, H. Kim, J. Lee, T. Badloe and J. Rho, Metasurface-empowered spectral and spatial light modu-

- lation for disruptive holographic displays, *Nanoscale*, 2022, **14**, 4380–4410.
- 17 H. Li, W.-B. Lee, C. Zhou, D.-Y. Choi and S.-S. Lee, Flat retroreflector based on a metasurface doublet enabling reliable and angle-tolerant free-space optical link, *Adv. Opt. Mater.*, 2021, **9**, 2100796.
 - 18 C. Zhou, W.-B. Lee, S. Gao, H. Li, C.-S. Park, D.-Y. Choi and S.-S. Lee, All-dielectric fiber meta-tip enabling vortex generation and beam collimation for optical interconnect, *Laser Photonics Rev.*, 2021, **15**, 2000581.
 - 19 K. Ou, F. Yu, G. Li, W. Wang, A. E. Miroschnichenko, L. Huang, P. Wang, T. Li, Z. Li, X. Chen and W. Lu, Mid-infrared polarization-controlled broadband achromatic metadvice, *Sci. Adv.*, 2020, **6**, eabc0711.
 - 20 S. Gao, C.-S. Park, S.-S. Lee and D.-Y. Choi, All-dielectric metasurfaces for simultaneously realizing polarization rotation and wavefront shaping of visible light, *Nanoscale*, 2019, **11**, 4083–4090.
 - 21 H. Altug, S. H. Oh, S. A. Maier and J. Homola, Advances and applications of nanophotonic biosensors, *Nat. Nanotechnol.*, 2022, **17**, 5–16.
 - 22 H. Li, J. T. Kim, J.-S. Kim, D.-Y. Choi and S.-S. Lee, Metasurface-incorporated optofluidic refractive index sensing for identification of liquid chemicals through vision intelligence, *ACS Photonics*, 2023, **10**, 780–789.
 - 23 T. Chantakit, C. Schlickriede, B. Sain, F. Meyer, T. Weiss, N. Chattham and T. Zentgraf, All-dielectric silicon metalens for two-dimensional particle manipulation in optical tweezers, *Photonics Res.*, 2020, **8**, 1435–1440.
 - 24 R. Geromel, R. Rennerich, T. Zentgraf and H. Kitzlerow, Geometric-phase metalens to be used for tunable optical tweezers in microfluidics, *Liq. Cryst.*, 2023, **50**, 1–11.
 - 25 T. Li, X. Xu, B. Fu, S. Wang, B. Li, Z. Wang and S. Zhu, Integrating the optical tweezers and spanner onto an individual single-layer metasurface, *Photonics Res.*, 2021, **9**, 1062–1068.
 - 26 X. Li, Y. Zhou, S. Ge, G. Wang, S. Li, Z. Liu, X. Li, W. Zhao, B. Yao and W. Zhang, Experimental demonstration of optical trapping and manipulation with multifunctional metasurface, *Opt. Lett.*, 2022, **47**, 977–980.
 - 27 S. Suwannasophon, F. Meyer, C. Schlickriede, P. Chaisakul, J. T-Thienprasert, J. Limtrakul, T. Zentgraf and N. Chattham, Miniaturized metalens based optical tweezers on liquid crystal droplets for lab-on-a-chip optical motors, *Crystals*, 2019, **9**, 515.
 - 28 M. Plidschun, H. Ren, J. Kim, R. Förster, S. A. Maier and M. A. Schmidt, Ultrahigh numerical aperture meta-fibre for flexible optical trapping, *Light: Sci. Appl.*, 2021, **10**, 57.
 - 29 L. J. Kong, W. Zhang, P. Li, X. Guo, J. Zhang, F. Zhang, J. Zhao and X. Zhang, High capacity topological coding based on nested vortex knots and links, *Nat. Commun.*, 2022, **13**, 2705.
 - 30 S. G. Reddy, S. Prabhakar, A. Aadhi, J. Banerji and R. P. Singh, Propagation of an arbitrary vortex pair through an astigmatic optical system and determination of its topological charge, *J. Opt. Soc. Am. A*, 2014, **31**, 1295–1302.
 - 31 J. Wen, B. Gao, G. Zhu, D. Liu and L. G. Wang, Precise position and angular control of optical trapping and manipulation via a single vortex-pair beam, *Opt. Lasers Eng.*, 2022, **148**, 106773.
 - 32 G. Indebetouw, Optical vortices and their propagation, *J. Mod. Opt.*, 1993, **40**, 73–87.
 - 33 Y. Fu, C. Min, J. Yu, Z. Xie, G. Si, X. Wang, Y. Zhang, T. Lei, J. Lin, D. Wang, H. P. Urbach and X. Yuan, Measuring phase and polarization singularities of light using spin-multiplexing metasurfaces, *Nanoscale*, 2019, **11**, 18303–18310.
 - 34 G. Li, B. P. Clarke, J. K. So, K. F. MacDonald and N. I. Zheludev, Holographic free-electron light source, *Nat. Commun.*, 2016, **7**, 13705.
 - 35 G. D'Aguanno, N. Mattiucci, M. Bloemer and A. Desyatnikov, Optical vortices during a superresolution process in a metamaterial, *Phys. Rev. A*, 2008, **77**, 043825.
 - 36 K. Ou, G. Li, T. Li, H. Yang, F. Yu, J. Chen, Z. Zhao, G. Cao, X. Chen and W. Lu, High efficiency focusing vortex generation and detection with polarization-insensitive dielectric metasurfaces, *Nanoscale*, 2018, **10**, 19154–19161.
 - 37 H. Li, C. Zhou, W.-B. Lee, D.-Y. Choi and S.-S. Lee, Flat telescope based on an all-dielectric metasurface doublet enabling polarization-controllable enhanced beam steering, *Nanophotonics*, 2021, **11**, 405–413.
 - 38 Z. Shi, M. Khorasaninejad, Y. W. Huang, C. Roques-Carmes, A. Y. Zhu, W. T. Chen, V. Sanjeev, Z.-W. Ding, M. Tamagnone, K. Chaudhary, R. C. Devlin, C.-W. Qiu and F. Capasso, Single-layer metasurface with controllable multiwavelength functions, *Nano Lett.*, 2018, **18**, 2420–2427.
 - 39 T. Li, F. Zi, K. Huang and X. Lu, Multifocus autofocusing Airy beam, *J. Opt. Soc. Am. A*, 2017, **34**, 1530–1534.
 - 40 T. Mu, Z. Chen, S. Pacheco, R. Wu, C. Zhang and R. Liang, Generation of a controllable multifocal array from a modulated azimuthally polarized beam, *Opt. Lett.*, 2016, **41**, 261–264.
 - 41 I. Koirala, S.-S. Lee and D.-Y. Choi, Highly transmissive subtractive color filters based on an all-dielectric metasurface incorporating TiO₂ nanopillars, *Opt. Express*, 2018, **26**, 18320–18330.
 - 42 I. Y. Kang, J. Ahn, Y. C. Chung and H. K. Oh, Aerial image characteristics of modified absorber model for extreme ultraviolet lithography (EUVL), *J. Korean Phys. Soc.*, 2008, **52**, 1759.